A Review on the Preparation of Borazine-Derived Boron Nitride Nanoparticles and Nanopolyhedrons by Spray-Pyrolysis and Annealing Process

Vincent Salles, Samuel Bernard

Nanomaterials and Nanotechnology

OPEN ACCESS
ARTICLE

A Review on the Preparation of Borazine-derived Boron Nitride Nanoparticles and Nanopolyhedrons by Spray-pyrolysis and Annealing Process

Invited Review Article

Vincent Salles[1] and Samuel Bernard[2]*

1 Laboratoire des Multimatériaux et Interfaces, Université Lyon, CNRS, France
2 IEM (Institut Europeen des Membranes), (CNRS-ENSCM-UM), Universite Montpellier, Montpellier, France
*Corresponding author(s) E-mail: Samuel.Bernard@umontpellier.fr

Received 05 October 2015; Accepted 15 December 2015

DOI: 10.5772/62161

Abstract

Boron nitride (BN) nanostructures (= nanoBN) are structural analogues of carbon nanostructures but display different materials chemistry and physics, leading to a wide variety of structural, thermal, electronic, and optical applications. Proper synthesis routes and advanced structural design are among the great challenges for preparing nanoBN with such properties. This review provides an insight into the preparation and characterization of zero dimensional (0D) nanoBN including nanoparticles and nanopolyhedrons from borazine, an economically competitive and attractive (from a technical point of view) molecule, beginning with a concise introduction to hexagonal BN, followed by an overview on the past and current state of research on nanoparticles. Thus, a review of the spray-pyrolysis of borazine to form BN nanoparticles is firstly presented. The use of BN nanoparticles as precursors of BN nanopolyhedrons is then detailed. Applications and research perspectives for these 0D nanoBN are discussed in the conclusion.

Keywords Borazine, Spray-Pyrolysis, Boron Nitride, Nanoparticles, Nanopolyhedrons, Annealing

Glossary

BN: Hexagonal Boron Nitride

t-BN: Turbostratic-BN

a-BN: Amorphous-BN

NPs: Nanoparticles

NPHs: Nanopolyhedrons

NCs: Nanocapsules

0D: Zero Dimensional

CNTs: Carbon Nanotubes

BNNTs: Boron Nitride Nanotubes

Borazine: BZ, $H_3B_3N_3H_3$

CVD: Chemical Vapor Deposition

SP: Spray-Pyrolysis

BET: Brunauer-Emmett-Teller

PDCs: Polymer-Derived Ceramics

H_3BO_3: Boric Acid

B_2O_3: Boric Oxide

$C_3H_6N_6$: with melamine

$CO(NH_2)_2$: Urea

$[C(NH_2)_3]_2[B_4O_5(OH)_4]\bullet 2H_2O$: Guanidinium Borate

$(MeO)_3B$: Trimethylborate

HBO_3: Hydrogen Borate

$Na_2B_4O_7$: Sodium Tetraborate Decahydrate

NH_4BF_4: Barberiite

NaN_3: Sodium Azide

NH_4Cl): Ammonium Chloride

CuO: Copper Oxide

$NaBH_4$: Sodium Borohydride

$(NH_4)_2SO_4$: Ammonium Sulfate

$FeCl_3$: Iron Trichloride

1. Introduction

Technological progress continuously calls for materials with optimized and novel advanced properties in which the functionality is controlled by nanoscale structures leading to improved and/or new applications [1]. In this category of advanced materials, inorganic compounds stimulate current research activities in many emerging topics ranging from fundamental science to applications such as in sustainable technology, energy conversion, and environmental issues. This is particularly the case for oxide ceramics. However, these materials do not always cover the current technological needs in some applications for which a chemical and/or thermal resistance is required [2,3]. Accordingly, there are growing efforts to prepare nonoxide ceramics that could extend the application of inorganic compounds and one of the most promising categories for that is nitride.

Nitride materials are nitrogen-containing inorganic compounds that contain the nitrogen ion N^{3-} (oxidation state of -3). Nitrides exist in two categories: the ionic-covalent family of nitrides and the transition metal series of the periodic table. In general, they are considered as refractory materials due to the fact that the nitrogen ion strongly attracts the relevant electrons in the chemical bond. Besides this, they display particular properties (electric insulation, thermal conductivity, hardness, etc.) according to their composition to provide an extremely large panel of functions. In the category of covalently bonded nitrides, hexagonal-boron nitride (*h*-BN but expressed here as BN) has recently attracted considerable attention in relation with its unique combination of key properties. It is considered in the present paper.

BN was discovered in the early 19th century and commercially developed in the latter half of the 20th century [4]. It consists of a layered structure with equal numbers of boron (B) and nitrogen (N) atoms linked by sp^2 hybridized orbits and held together mainly by Van der Waals force [5]. Because BN is isostructural to carbon (C) forming a honeycomb-like network analogous to graphite, the researches focused on BN are in general linked to the works performed on carbon. In particular, interest at the academic level has arisen in the synthesis of nanostructured BN (= nanoBN). As an illustration, the discovery of carbon nanotubes (CNTs) by Iijima in 1991 [6] encouraged intense experimental and theoretical research investigations on their BN analogues (= BN nanotubes, BNNTs) [7]. Similarly, the formation of BN fullerenes [8] was inspired by the first fullerene molecule, the buckminsterfullerene (C_{60}), reported in 1985 [9]. Afterward, the discovery of graphene in 2004 [10] inspired researches on their 2D BN counterparts [11]. Finally, like carbon, the layered structure of BN provides useful properties and its modification by various post-synthesis treatments has attracted considerable attention recently [12-19].

BN displays good lubricating properties according to its layered structure (weakly held layers can slide over each other). It proposes a very high thermal conductivity (in the direction of hexagons), a high thermal stability, a high resistance to corrosion and oxidation, as well as a strong UV emission [20-23]. It offers high dielectric breakdown strength and high volume resistivity. BN displays a large band gap (~5.5 eV) and offers the lowest density (d = 2.26 g cm^{-3}) among nonoxide ceramics. In addition, it can provide superhydrophobicity depending on its shape and synthesis procedure [24-25]. Furthermore, the local polar character of the B-N bonds is present in the BN structure. As an illustration, BN has been demonstrated to exhibit enhanced sorption properties of various substances such as organic pollutants [25-31] and hydrogen [31-34]. However, these properties vary drastically with the synthesis route employed to prepare BN.

BN was synthesized by Balmain [35] in 1842, applying the reaction between molten boric acid (H_3BO_3) and potassium cyanide (KCN). It is nowadays produced by conventional powder technology, requiring nitridation or carbothermal reaction of boric acid (H_3BO_3)/boric oxide (B_2O_3) with melamine ($C_3H_6N_6$) or urea ($CO(NH_2)_2$) and the use of additives during the further sintering process [36]. BN is used in various fields of chemistry, metallurgy, high-temperature technology, electronic and in thermal management applications. However, the design of BN in which the structure is designed at nanoscale to generate nanoBN such as nanoparticles (NPs) is complex to investigate for future industrial challenges. Proper synthesis routes and advanced structural design are among the great challenges for preparing nanoBN.

Among the category of nanoBN, NPs have received less attention than BNNTs despite their wide-spectrum uses (as

functional materials for high thermal conductivity and electrically insulating composites or as precursors for others materials). In the present paper, we have restricted ourselves to the synthesis of BN NPs starting with a state-of-the-art focused on BN particles and NPs. It is followed by the preparation and characterization of borazine-derived BN NPs in particular using spray-pyrolysis, and the thermal behavior of the BN NPs at high temperature leading to generate BN nanopolyhedrons (NPHs).

2. General Routes for the Preparation of BN Particles and NPs

The first intensive efforts on the preparation of BN particles and submicronic particles were made by Paine *et al.* [37-41]. Firstly, they used an aerosol-assisted vapor synthesis (Figure 1) from liquid ammonia solutions of poly(borazinylamine) to provide BN particles. However, this route was considered to be not convenient and relatively expensive [37].

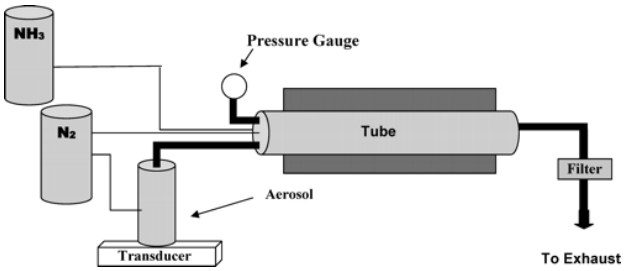

Reproduced with permission from ACS

Figure 1. Schematic diagram of the aerosol process [39]

Later, they investigated the same process using aerosol droplets containing water-soluble H_3BO_3 at 1200°C in an ammonia/nitrogen atmosphere [38]. The particles were spherical and displayed a diameter of 1–2 µm. In 2005, the same authors were able to reduce the size of BN particles through the pyrolysis of aqueous aerosols containing a guanidinium borate ($[C(NH_2)_3]_2[B_4O_5(OH)_4]\bullet 2H_2O$) under ammonia/nitrogen flow up to 1600°C [39]. One year later, Paine *et al.* used trimethylborate ($(MeO)_3B$) in neat form in methanol as an aerosol precursor to produce, by reaction with ammonia, spherical BN particles with a high production rate, low oxygen and carbon contents (as a consequence of a post-pyrolysis annealing at 1600°C), and with a diameter 0.2–2 µm (Figure 2) [40]. These BN powders could be prepared as mesoporous materials [41].

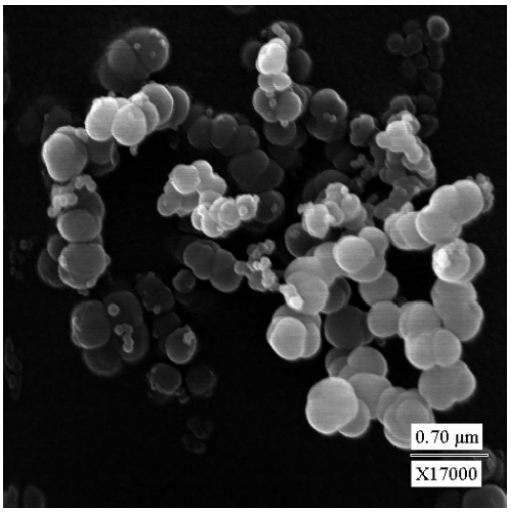

Reproduced with permission from ACS

Figure 2. SEM image of BN particles produced from $(MeO)_3B$ aerosol and post-pyrolyzed at 1600°C [40]

Bando *et al.* prepared submicronic spherical BN particles with diameters ranging from 50 to 400 nm (Figure 3) by using a two-step synthetic process [42-43].

They combined chemical vapor deposition of solutions of $(MeO)_3B$ under ammonia using two types of systems (Figure 4) and annealing treatment. Authors showed that they could generate two types of BN particles according to the used CVD systems: using ammonia at 1400°C during annealing, oxygen-containing BN with a diameter around 90 nm and BET Specific Surface Area (SSA) of 26.8 m²/g

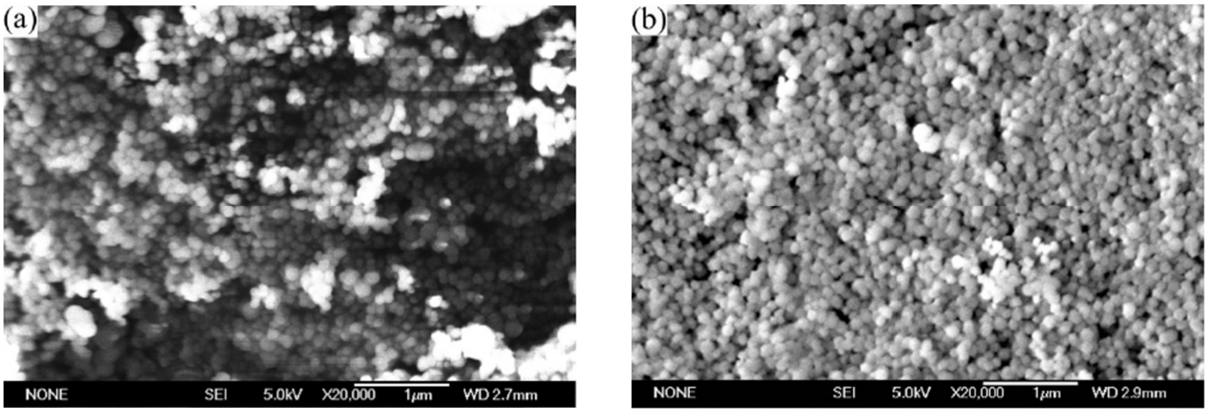

Reproduced with permission from RSC

Figure 3. SEM image of BN particles synthesized by CVD of $(MeO)_3B$ (a) then annealed at 1100°C (b) [42]

could be obtained. Oxygen-free BN particles with a diameter of 30 nm and at BET SSA of 52.7 m^2/g could be generated using argon instead of ammonia during the annealing process [43]. Following a two-step process, Shi *et al.* synthesized BN particles in the diameter range 0.5–1.5 μm by spray-drying a mixture of hydrogen borate (HBO_3), Sodium tetraborate decahydrate ($Na_2B_4O_7$) at 250°C which was subsequently mixed with $(NH_2)_2CO$ to be heated in air at 900°C. As-made particles were nitrided at different temperatures from 1200 to 1550 °C [44]. In 2010, monodisperse BN NPs were prepared by a modified solid-state reaction route, using barberiite (NH_4BF_4) and sodium azide (NaN_3) as the reactants. As-prepared BN NPs displayed good thermal stability and high specific surface area [45]. More recently, BN NPs with diameters from 20 to 100 nm have been prepared from B_2O_3 by high-energy ball-milling followed by annealing at 1200°C [46]. These NPs were mainly elliptical plate-like with diameters ranging from 20 to 100 nm. Impurities were detected. In a last report, Xiong *et al.* produced water-dispersible BN NPs with diameter of around 30 nm by direct reaction of H_3BO_3 and ammonium chloride (NH_4Cl) [47]. Copper oxide (CuO) has been identified in the final product.

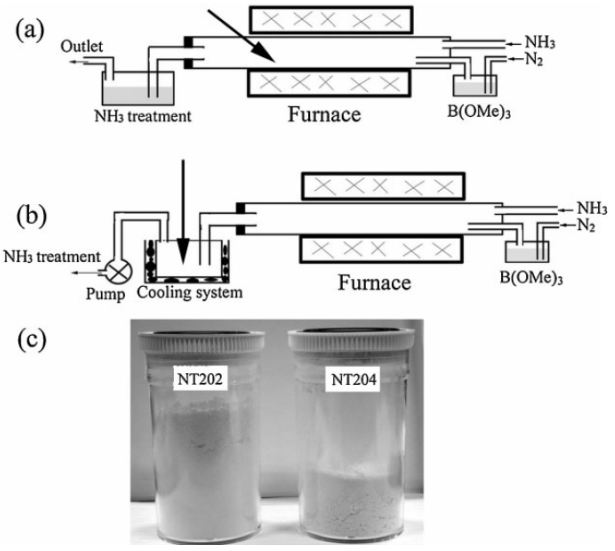

Reproduced with permission from Wiley

Figure 4. Schematic diagram of the synthetic systems used in the traditional (leading to samples labeled NT204) (a) and modified CVD processes (leading to samples labeled NT202) (b), and the appearance of the samples NT202 and NT204 [43] (c). Arrow points to the area of the sample

Based on the previously described studies, it appears that the selection of the BN precursor is important to avoid impurities in the final materials. It is clear that precursors with the stoichiometric B:N ratio and the preformed B_3N_3 ring, while hydrogen (H) is the only element added to B and N, are required to prepare BN. Borazine (BZ, $H_3B_3N_3H_3$) appears to be an appropriate precursor of BN NPs. Borazine-derived BN NPs have been reported by Hidalgo *et al.* [48]. In particular, they described the formation of BN NPs (mixed with cubic BN NPs) using laser CVD. However, few data have been provided concerning the nanostructure of these materials. Besides this report, our group demonstrated in 2009 the possibility to produce pure BN NPs from the spray-pyrolysis of BZ [49], which is the subject of the next section.

3. Spray-pyrolysis Process of Borazine – Preparation of BN NPs

3.1 Synthesis and Characterization of Borazine

BZ represents a highly pure synthetic low-molecular weight precursor with the planar six-numbered hexagonal ring in which uniform chemical composition is established at the molecular scale [50]. BZ is isolectronic and isostructural of benzene and has the chemical formula $H_3B_3N_3H_3$. BZ was first isolated by Alfred Stock in 1926 [51]. It displays a melting point of -58 °C and a boiling temperature of +55 °C.

BZ can be used as a BN precursor following two strategies. In a first strategy, it can be polymerized into a macromolecule (= inorganic or preceramic polymer called polyborazylene) by self-condensation; then this polymer offers many opportunities to produce BN (with a control of the composition at the molecular scale) in various morphologies and porosities following the Polymer-Derived Ceramics (PDCs) route [52-58]. BZ offers the advantage of being a colorless liquid with an adequate vapor pressure. As a consequence, it can be used in a second strategy in various vapor-phase processes [48,59-65]. In the present section, the preparation of BZ-derived BN NPs by spray-pyrolysis is reported from the synthesis and characterization of BZ to the characterization and high-temperature thermal behavior of BN NPs. In the following section, their use as precursors for preparing nanopolyhedrons (NPHs) [66-67] has been selected for discussion.

First of all, BZ can be prepared through different pathways with probably the most economical one being from sodium borohydride ($NaBH_4$) and ammonium sulfate ($(NH_4)_2S0_4$) [68]. The ^1H NMR of BZ consists of a BH quadruplet between 3.40 and 5.20 ppm and an NH triplet between 5.20 and 5.95 ppm (Fig. 5a).

The IR spectrum in Fig. 5b is consistent with the formation of BZ: it is dominated by the $\nu_{B\text{-}H}$ (2515 cm^{-1}), the characteristically sharp $\nu_{N\text{-}H}$ (3452 cm^{-1}), the B-N stretch near 1445 cm^{-1}, and the B-N-B bending mode at ~900 cm^{-1}; the two last bands are characteristic of the borazine ring [69-70]. The deformation of N-H bending is characterized by the band at ~715 cm^{-1}, whereas the small band emerging around 1170 cm^{-1} could be attributed to B-H bending [71]. As previously mentioned, BZ is volatile and can be used in a spray-pyrolysis (SP) apparatus to produce NPs.

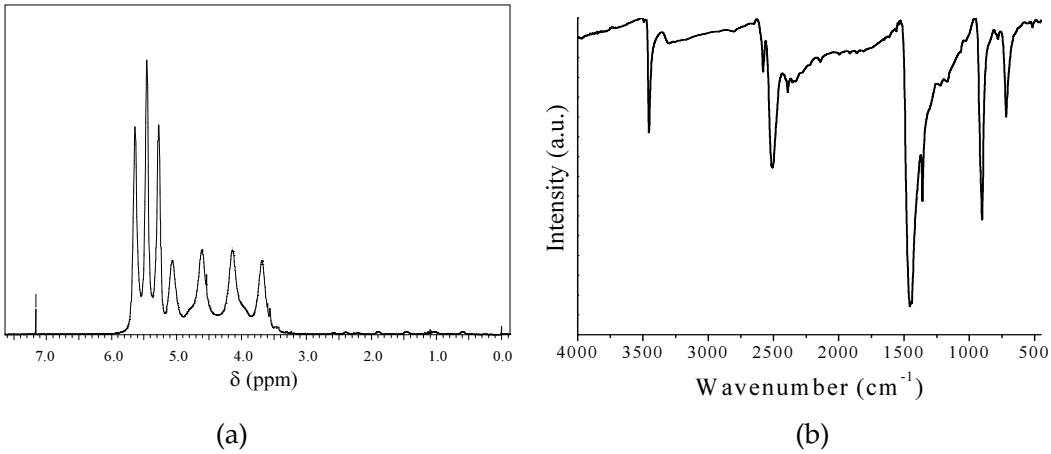

Figure 5. (a) ^{1}H NMR spectrum recorded in $CDCl_3$ and (b) FTIR spectrum of BZ

3.2 Spray-pyrolysis of Borazine and Preparation of BN NPs

SP is a method in which a precursor is delivered as an aerosol, *i.e.*, tiny droplets carried by nitrogen. Then, the precursor droplets are carried by a gas and the aerosol is carried out in a pyrolysis reactor to be converted into solid nanoparticles. Here, BZ droplets are carried out by nitrogen into the pyrolysis reactor fixed at 1400 °C to be fully evaporated (according to their relatively high vapor tension) and decomposed into BN powders that are collected in two traps. Nucleation from the vapor phase and growth of BZ are involved in the process of nanoparticle formation. Figure 6 presents the SP process using BZ to produce BN NPs.

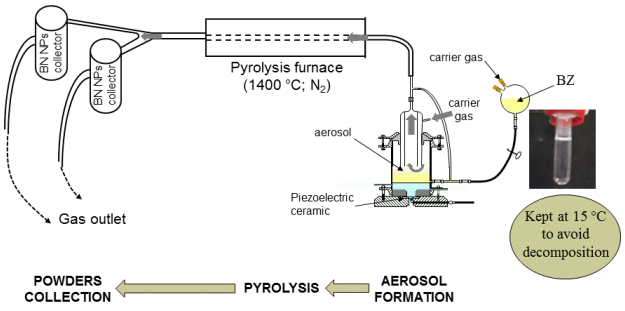

Figure 6. Schematic diagram of the spray-pyrolysis of BZ leading to BN NPs

3.3 (Nano)structural Characterization of BN NPs

The XRD pattern and the solid-state ^{11}B NMR spectrum of as-obtained powders are presented in Fig. 7. The XRD pattern of commercially available BN is in general composed of peaks at 26.76° (002), 41.60° (100), 43.87° (101), 50.15° (102), 55.16° (004), 75.93° (110), 82.18° (112), and 85.52° (105) [72]. However, it is extremely difficult to form the hexagonal phase of BN and to identify all the peaks characteristic of this phase in the XRD pattern of precursor-derived BN. Two disordered BN phases, turbostratic-BN (*t*-BN), and amorphous-BN (*a*-BN), are in general identified [73-75]. *t*-BN shows a random stacking sequence of the (002) layers and a disorientation of these layers around the *c*-axis. *a*-BN represents a structure disordered at atomic level. XRD patterns of such phases are significantly distinct from that of BN. This is the case of BZ-derived powders. As an illustration, the XRD pattern of powders showed broadened (002) peaks and diffuse (100 and 110) peaks which are significantly shifted to the Bragg angles of BN [49]. The pattern of BZ-derived powders is representative of a *t*-BN structure. The formation of *t*-BN most probably results from the SP process. The extremely fast heating rate involved by this SP process (~10^2 °C/s) associated with the short residence time of BZ at 1400°C (3 s) inherently leads to the low crystallization of BN powders. We investigated solid-state ^{11}B NMR of powders. ^{11}B solid-state NMR spectrum of the sample (Fig. 7 inset) shows a large signal in the region of tricoordinated boron atoms that could be assigned to B–N bonds in planar BN_3 groups [54,56] within BN graphitic layers. The second small signal at δ = 0.6 ppm (no quadrupolar shape) is indicative of the presence of tetragonal BO_4 groups [76-77] in a low portion.

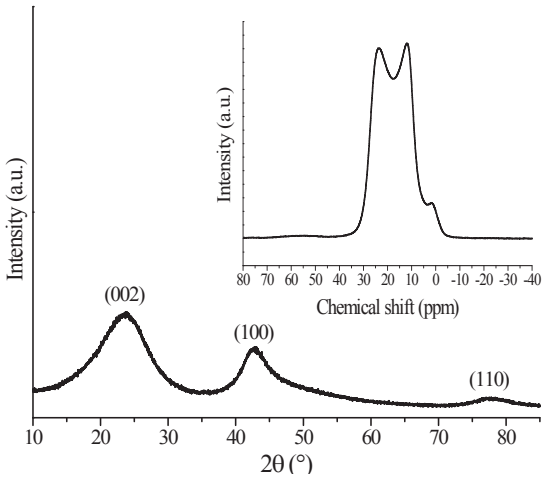

Figure 7. XRD pattern and ^{11}B NMR spectrum of BN NPs prepared by spray-pyrolysis of borazine at 1400°C

Transmission Electron Microscopy (TEM) was investigated to estimate locally the size of powders as well as their agglomeration level and to confirm their low degree of crystallization. The low-magnification TEM bright field image of BN powders (Fig. 8) showed that samples are composed of agglomerated NPs, but their easy dispersion in solvent proved that agglomeration level is low. The particle population was relatively homogeneous and the NP size ranged from 55 to 120 nm [49]. Data provided by the corresponding selected area electron diffraction (SAED) pattern, inset in Figure 8 highly reflected XRD results. The amorphous halo imposed on the diffuse and continuous (002) arcs and the poorly resolved (004) ring confirm the low level of crystallinity of BN NPs [79].

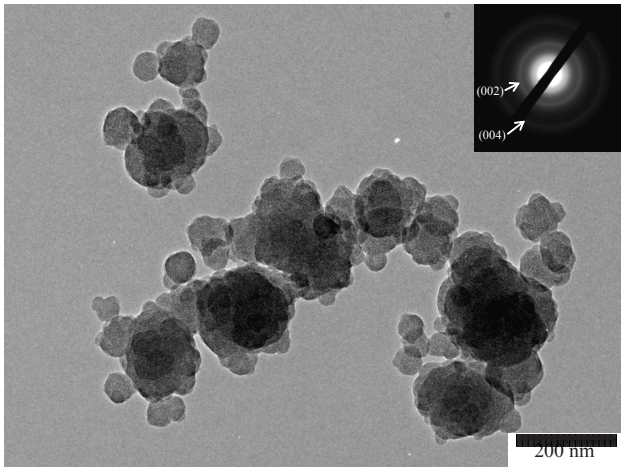

Figure 8. TEM micrographs and SAED pattern of BN NPs prepared by spray-pyrolysis of BZ at 1400°C

The high-resolution TEM (HRTEM) image (Fig. 9) showed that the long-range ordering is minimal and the crystallinity is inhomogeneous. The lattice image in Fig. 9 highlighted the presence of grains with a low thickness and layers with high tortuosity in their stacking sequence as commonly observed in precursor-derived BN [80-81]. It was interesting to observe that a certain portion of the smallest particles (≤10 nm) seems to be hollow.

3.4 Characterization at the Mesoscopic Scale of BN NPs

The NPs have been characterized at the mesoscopic length scale by nitrogen gas adsorption–desorption measurement at 77 K [49]. Based on IUPAC classification [82-83], the adsorption–desorption isotherms of the BN NPs (Fig. 10) depict a type-I/II shape, which strongly suggests the formation of nonporous NPs, which was confirmed by the low BET SSA of samples (<35 m²/g). However, the adsorption hysteresis of type H4 could indicate the presence of micropores in the NPs.

3.5 Characterization of BN NPs by XPS

In the present paper, the chemical environment around the B, N, C, and O atoms in powders has been investigated by

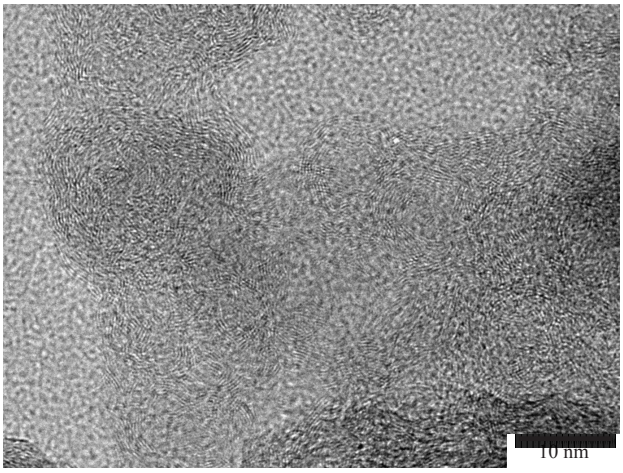

Figure 9. HRTEM micrographs of BN NPs prepared by spray-pyrolysis of BZ at 1400°C

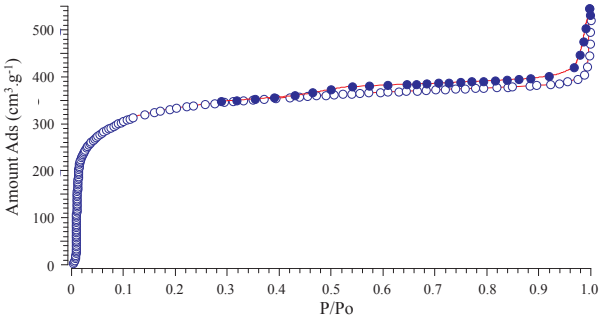

Figure 10. N_2 adsorption–desorption isotherms recorded at 77 K of BN NPs prepared by spray-pyrolysis of BZ at 1400°C

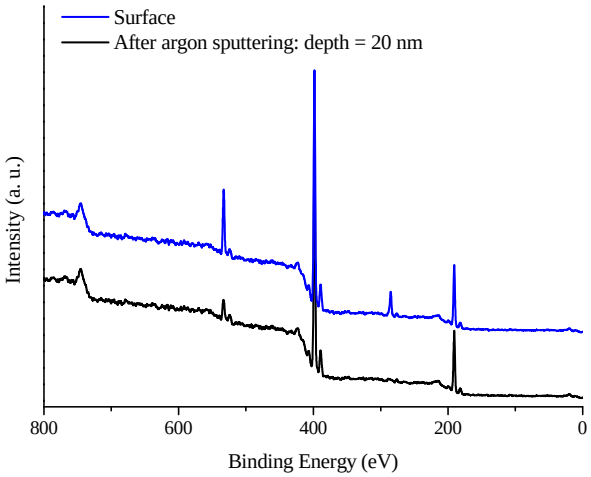

Figure 11. XPS spectra from BN NPs prepared by spray-pyrolysis of BZ at 1400°C after argon sputtering corresponding to a depth profile of 20 nm

X-ray Photoelectron Spectroscopy (XPS). Figure 11 displays the general XPS graphs recorded on the surface and after argon sputtering and Fig. 12 reports the characteristic individual peaks attributed to B 1s and N 1s environments. Figure 11 shows that XPS spectroscopy is oversensitive to surface groups: BN powders are very

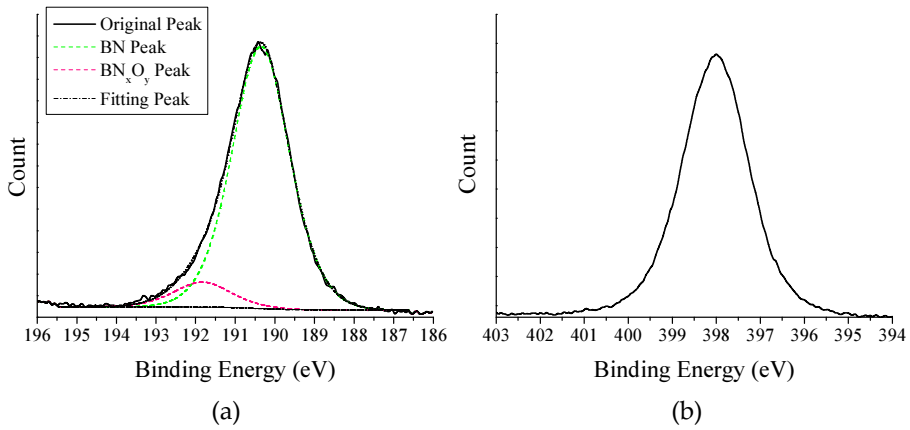

Figure 12. High-resolution B 1s (a), (b) N 1s XPS spectra of BN NPs prepared by spray-pyrolysis of BZ at 1400°C

prone to surface passivation with atmospheric oxygen. The detection of carbon and oxygen, which are considerably reduced after argon sputtering, clearly results from contamination. XPS results (B, 41.6 at%; N, 41.2 at%; C, 9.0 at%; O, 8.2 at%) for the surface of the sample give evidence that the bulk composition of the material is close to stoichiometric BN. The B 1s peak at 190.8 eV corresponds to the B-N bonding, whereas the one at 191.9 eV (Fig. 12a, only at the surface of the bulk sample) corresponds to B_2O_3 [78]. The N 1s peak (Fig. 12b) at 398 eV is typical for nitrogen shifts in BN [55]. However, we can suggest that contamination is extremely low and the SP process of BZ leads to pure BN NPs.

3.6 High-temperature Behavior of BN NPs by XPS

Because the BN NPs displayed a low degree of crystallinity, we investigated their behavior at high temperature in the temperature range 1000–1800°C under nitrogen atmosphere (Figure 13) [66-67], especially their weight change by High-Temperature ThermoGravemetric Analysis (HT-TGA). In addition, we investigated the same high-temperature range under argon. The profile of both curves is similar: BN NPs underwent a first weight loss from RT to 800°C, followed by a plateau from 800 to 1100°C, and then a second weight loss was identified.

As previously suggested, the conversion of BZ into BN is not fully achieved by SP and some hydrogen atoms remain at the periphery of the BN network. Therefore, we suggested that the first weight loss identified in Fig. 13 results from evolution of residual hydrogen. It represents 1.2% of weight loss. The second weight loss is more complex to interpret, whereas BN is known to be stable up to 2000°C as shown in our previous paper [67]. We concluded that it probably results from the poor crystallinity of BN NPs. Within this context, we have investigated the structural evolution on BN NPs by heat-treatment under nitrogen in the temperature range 1400–1800°C, leading to the formation of the materials we labeled **BNNP1600** (BN NPs annealed at 1600°C), **BNNP1700** (BN NPs annealed at 1700°C), **BNNP1800** (BN NPs annealed at 1800°C) [66-67]. Because BN is expected to be stable up to 2000°C under nitrogen, a sample pyrolyzed at 2000°C, *i.e.*, **BNNP2000**, has been also analyzed in the present paper in complement to other samples. This annealing leads to the formation of BN nanopolyhedrons (NPHs), which are discussed in the following section.

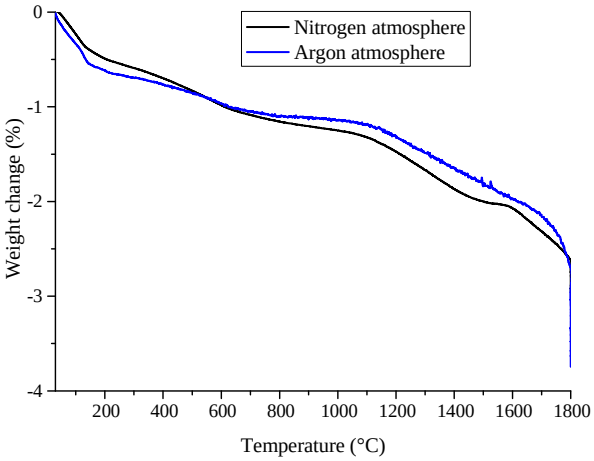

Figure 13. HT-TGA of of BN NPs prepared by spray-pyrolysis of BZ at 1400°C (RT-1800°C, argon and nitrogen atmospheres)

4. Annealing of BZ-derived BN NPs – Preparation of BN NPHs

Interestingly, the heat-treatment of BN NPs in the temperature range 1400–2000°C modified their nano-/microstructure as shown on the TEM images of samples **BNNP1600**, **BNNP1700**, **BNNP1800,** and **BNNP2000** (Fig. 14). As already observed for BN NPs, low-magnification TEM images show that the annealed samples form blocks that are composed of agglomerated NPs. It seems that agglomeration increases with the annealing temperature, whereas the size of the nanoparticles decreases. The HRTEM images highlighted the effect of the annealing temperature on the crystallization degree.

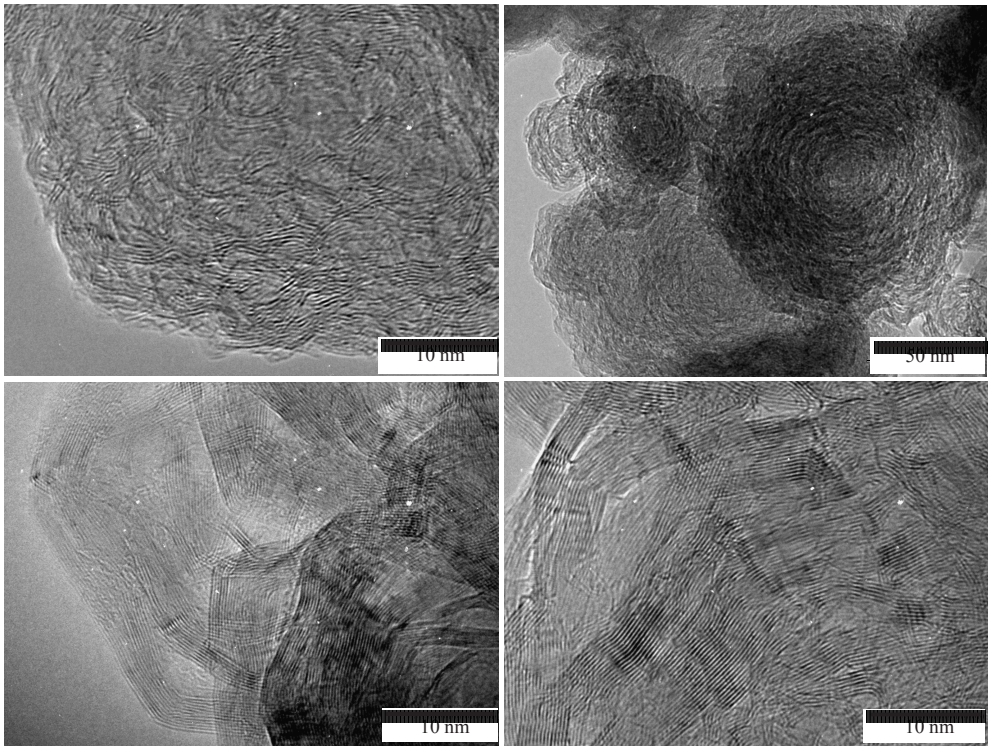

Figure 14. High-magnification TEM bright field images of the samples **BNNP1600**, **BNNP1700**, **BNNP1800**, **BNN**P2000

It should be mentioned that the NPs annealed at 1450°C did not show strong differences in comparison to as-obtained BN NPs. In contrast, in the sample **BNNP1600**, concentric rings are gradually formed and we observe that BN layers tend to be arranged forming hollow core-shell structures as evidenced in Fig. 14a within a nanoparticle.

A similar arrangement of the BN layers is identified, *i.e.*, formation of hollow core-shell structures, in the sample **BNNP1700** (Fig. 14b), but here it seems that small NPs are agglomerated around bigger one forming flower-like architectures.

The flower-like architecture was kept after annealing the BN NPs at 1800°C (**BNNP1800**) and 2000°C (**BNNP2000**). However, we could observe at the periphery of the flower-like architectures the formation of strongly facetted hollow particles forming hollow nano-polyhedral shapes (Fig. 14c and d). The high-magnification image indicates that these NPHs are highly crystallized with an interlayer spacing of 3.34 Å. We proposed a mechanism leading to the formation of these NPHs [66]: We suggested that the NPHs' growth process was related to the surface free energy. The NPH configuration probably represents a minimum of energy for the set of configurations which could be available to the system.

There are some reports focused on the polyhedral morphology. Polyhedral BN-nanocapsules (BN-NCs) less than 80 nm in size have been synthesized by nitridation of Fe–B NPs obtained by reaction between $NaBH_4$ and Iron trichloride ($FeCl_3$) and treatment at 900°C under ammonia/nitrogen [84]. Treatment of the as-prepared product with dilute nitric acid (HNO3) was required to dissolve the Fe–B NPs and generate the polyhedral BN-NCs. Finally, most of the BN-NCs encapsulate nonmetallic, oxide or nitride NPs to form hybrid materials [85-89]. Therefore, the encapsulated particles need to be removed to obtain NPHs, which usually requires a complex purification process. Facile formation of hollow BN powders with spherical primary particle morphology has been achieved through an aerosol process [41,90]. However, such powders were produced at the microscale and the heat-treatment did not allow the formation of NPH structures. It is clear that the above conventional synthetic methods are not fitted to the synthesis of NPHs, especially with hollow cores. Here, the structural organization of the BN NPs produced by SP of BZ allowed the developing of a convenient route for the synthesis of gramscale BN NPHs at high temperature.

5. Experimental Part

5.1 Materials

The synthesis of BZ was carried out in an argon atmosphere, using argon/vacuum lines, and Schlenk-type flasks. Argon (>99.995%) was purified by passing through successive columns of phosphorus pentoxide (Sigma-Aldrich, Saint Quentin, France), sicapent (Millipore S.A.S, Molsheim, France), and copper-oxide-based catalysts (Sigma-Aldrich, Saint Quentin, France). Schlenks were dried at 120°C overnight before pumping under vacuum and filling them with argon for the synthesis. Sodium

borohydride ($NaBH_4$, ≥ 98.5%, powder from Sigma-Aldrich, Saint Quentin, France), ammonium sulfate ($(NH_4)_2SO_4$, ≥ 99.0% from Sigma-Aldrich, Saint Quentin, France), and tetraethylene glycol dimethyl ether ($CH_3O(CH_2CH_2O)_4CH_3$, 99.0 % from Sigma-Aldrich, Saint Quentin, France) were used as-received. It should be mentioned that ammonium sulfate was dried at 120°C inside an oven for three days, then put under vacuum during cooling for 1 h. Manipulation of the chemical products was made inside an argon-filled glove box (Jacomex BS521; Dagneux, France) dried with phosphorus pentoxide.

5.2 Synthesis of Borazine

The operating procedure, adapted from the literature [68], is reported in our previous paper [52].

5.3 Synthesis of BN NPs

The experimental setup (Fig. 6) is composed of a nebulized spray generator (RBI, Meylan, France), in which the spray is generated by a piezoelectric device (barium titanate). Frequency (800 kHz) and power (100 W) alimentations are adjusted to obtain the aerosol. The aerosol temperature is first held at 15°C by a regulated water circulation to avoid borazine evaporation and/or condensation. The piezoelectric device generates an ultrasound beam, which is directed to the liquid–gas interface; a fountain formed at the surface followed by the generation of the spray resulting from vibrations at the liquid surface and cavitations at the gas–liquid interface. BZ was directly introduced in the aerosol-generating chamber under nitrogen, then aerosolized and carried to the pyrolysis furnace with a 0.5 mL min^{-1} nitrogen flow rate. The thermal decomposition of borazine was performed in a hot alumina tube containing an isothermal zone of 0.1 m in length. The fast heating rate implies gaseous species generation leading to powder formation by a chemical vapor condensation route. The particles were finally trapped into two collectors placed before the vacuum pump and containing filter-barriers made of microporous alumina (pore size of 1 μm). Yield was estimated to be 0.22 g min^{-1}. After their synthesis, powders were stored inside an argon-filled glove-box. In a typical experiment, 27 mL (21.9 g) of BZ are used to produce 6.5 g of white-color powders. However, the exact yield is difficult to estimate because of the design of the SP system. A nonnegligible quantity of powders, deposited in the furnace tube, could not be recovered.

5.4 Characterization

FTIR spectrum of BZ was recorded from a Nicolet Magna 550 Fourier transform-infrared spectrometer by introducing the liquid molecule between two KBr windows. ^1H NMR spectrum were obtained using a Bruker AM 300 spectrometer in $CDCl_3$ operating at 300 MHz. Tetramethylsilane (TMS) was used as a reference for the NMR data. The XPS measurement of the final product was performed on a Perkin-Elmer PHI Quantera SXM multifunctional X-ray photoelectron spectroscope (Physical Electronics, USA), using Al-Kα radiation (photon energy 1476.6 eV) as the excitation source and the binding energy of Au (Au $4f_{7/2}$: 84.00 eV) as the reference. BN NPs and NPHs were characterized and analyzed by a transmission electron microscopy (TEM) with a TOPCON 002B working at 200 kV. Samples were characterized using a Philips PW 3040/60 X'Pert PRO X-ray diffraction system. Powder samples were prepared by placing ~100 mg on the XRD sample holder (PVC). Cu Kα (λ = 1.54 Å) radiation with an Ni filter was used with a working voltage and a current of 40 kV and 30 mA, respectively. Scans were continuous from 10-85° 2θ for powders with a time per step of 0.85 s in increments of 0.017° 2θ. Peak positions and relative intensities were characterized by comparison with JCPDS files of the standard material (JCPDS card No 34-0421). The Specific Surface Area (SSA) of BN NPs was measured on a Micromeritics-ASAP 2010, BET 8 pts. Samples (450 mg) were degassed at 250°C for 12 h. Analysis was run at 77 K with N_2. The BET specific surface area was calculated from the nitrogen adsorption data in the relative pressure range from 0.05 to 0.3. BN NPs were studied by high-temperature thermogravimetric analysis (HT-TGA, Setaram Setsys evolution TGA equipment) in argon and nitrogen atmospheres (50–1800°C; heating rates: 5°C/min) using tungsten crucibles.

6. Conclusions

This article reviews our recent advancements in the synthesis of 0D nanoBN, including nanoparticles (NPs) and nanopolyhedrons (NPHs) by spray-pyrolysis of borazine leading to BN NPs followed by the annealing of the latter to form NPHs at high temperature. In this review, we discussed the synthesis and characterization of borazine. Borazine offers the advantage of being a colorless liquid with an adequate vapor pressure, which is used as a spray-pyrolysis precursor for the synthesis of BN NPs. The extremely fast heating rate involved by this SP process (~10^2 °C/s), and the short residence time of borazine at 1400°C (3 s) led to BN NPs with a low crystallization degree, a size ranging from 55 to 120 nm and a low specific surface area (SSA). Through annealing at high temperature under nitrogen, BN NPs underwent two weight losses. The first weight loss up to 1100°C was associated with evolution of hydrogen, whereas the second weight loss above 1100°C was associated with a gradual change in the morphology of NPs from BN NPs to BN NPHs. The production of BN NPs by spray-pyrolysis of borazine is a necessary step in forming at 1400°C under nitrogen disordered BN NPs from which the BN NPHs may grow *via* a solid-state process in the temperature range 1400–2000°C. It is envisaged that these structures might open new opportunities in exploring chemical and physical properties. We consider that these BN architectures could find applications in many areas of

modern science and technology including adsorbents, optoelectronic devices, energy storage media as we recently demonstrated [34, 91], and catalyst support.

7. Acknowledgements

The authors acknowledge Prof. Sylvie Foucaud for the spray-pyrolysis investigation and Prof. Arnaud Brioude for the TEM observation of nanoparticles and samples annealed in the temperature range of 1450–2000°C. Dr. Samuel Bernard thanks University of Montpellier for providing financial support through the project entitled "Le nitrure de bore pour des applications « energie »" (2011, PP Energie type, Pole Chimie).

8. References

[1] Bechelany M C, Proust V, Gervais C, Ghisleny R, Bernard S, Miele P (2014) In-situ Controlled Growth of Titanium Nitride in Amorphous Silicon Nitride: A General Route Toward Bulk Non-Oxide Nitride Nanocomposites with Very High Hardness. Adv. Mater. 26: 6548–6553.

[2] Salameh C, Bruma A, Malo S, Demirci U B, Miele P, Bernard S (2015) Monodisperse Platinum Nanoparticles Supported on Highly Ordered Mesoporous Silicon Nitride Nanoblocks: Superior Catalytic Activity for Hydrogen Generation from Sodium Borohydride. RSC Adv. 5: 58943–58951.

[3] Majoulet O, Salameh C, Schuster M.E, Demirci U.B, Sugahara Y, Bernard S, Miele P (2013) Synthesis of Periodic Mesoporous Silicon-Aluminum-Carbon-Nitrogen Frameworks Surface-Decorated with Pt Nanoparticles. Chem. Mater. 25: 3957–3970.

[4] Paine R T, Narula C K (1990) Synthetic Route to Boron Nitride. Chem. Rev. 90: 73–91.

[5] Han W Q (2008) Anisotropic Hexagonal Boron Nitride Nanomaterials: Synthesis and Applications. Wiley-VCH Verlag GmbH & Co. KGaA: Weinheim, Germany, 2010.

[6] Iijima S (1991) Helical Microtubules of Graphitic Carbon. Nature 354: 56–58.

[7] Chopra N G, Luyken R J, Cherrey K, Crespi V H, Cohen M L, Louie S G, Zettl A (1995) Boron Nitride Nanotubes. Science 269:966–967.

[8] Stephan O, Bando Y, Loiseau A, Willaime F, Shramchenko N, Tamiya T, Sato, T (1998) Formation of Small Single-Layer and Nested BN Cages under Electron Irradiation of Nanotubes and Bulk Materials. Appl. Phys. A: Mater. Sci. Process 67:107–111.

[9] Kroto H W, Heath J R, O'Brien S C, Curl R F, Smalley R E (1985) C_{60}: Buckminsterfullerene. Nature 318:162–163.

[10] Novoselov K S, Geim A.K, Morozov S V, Jiang D, Zhang Y, Dubonos S V, Grigorieva I V, Firsov A A (2004) Electric Field Effect in Atomically Thin Carbon Films. Science 306: 666–669.

[11] Corso M, Auwarter W, Muntwiler M, Tamai A, Greber T, Osterwalder J (2004) Boron Nitride Nanomesh. Science 303:217–220.

[12] Wu Q, Jang S K, Park S, Jung S J, Suh H, Lee Y H, Lee S, Song, Y J. (2015) In-situ Synthesis of a Large Area Boron Nitride/Graphene Monolayer/Boron Nitride Film by Chemical Vapor Deposition. Nanoscale 7:7574–7579.

[13] Lin Y, Connell J W (2012) Advances in 2D Boron Nitride Nanostructures: Nanosheets, Nanoribbons, Nanomeshes, and Hybrids with Graphene. Nanoscale 4:6908–6939.

[14] Shin H C, Jang Y, Kim T H, Lee J H, Oh D H, Ahn S J, Lee J H, Moon Y, Park J H, Yoo S J, Park C Y, Whang D, Yang C W, Ahn J.R (2015) Epitaxial Growth of a Single-Crystal Hybridized Boron Nitride and Graphene Layer on a Wide-Band Gap Semiconductor. J. Am. Chem. Soc. 137:6897–6905.

[15] Parra C, Montero-Silva F, Henríquez R, Flores M, Garín C, Ramírez C, Moreno M, Correa J, Seeger M, Häberle P (2015) Suppressing Bacterial Interaction with Copper Surfaces through Graphene and Hexagonal-Boron Nitride Coatings. ACS Appl. Mater. Interf. 7:6430–6437.

[16] Lu J, Gomes L C, Nunes R W, Castro Neto A H, Loh K P (2014) Lattice Relaxation at the Interface of Two-Dimensional Crystals: Graphene and Hexagonal Boron-Nitride. Nano. Lett. 14:5133–5139.

[17] Lee D, Lee B, Park K H, Ryu H J, Jeon S, Hong S H (2015) Scalable Exfoliation Process for Highly Soluble Boron Nitride Nanoplatelets by Hydroxide-Assisted Ball Milling. Nano. Lett. 15:1238–1244.

[18] Morishita T, Okamoto H, Katagiri Y, Matsushita M, Fukumori K (2015) A High-Yield Ionic Liquid-Promoted Synthesis of Boron Nitride Nanosheets by Direct Exfoliation. Chem. Comm. 51:12068–12071.

[19] Marsh K L, Souliman M, Kaner R B (2015) Co-Solvent Exfoliation and Suspension of Hexagonal Boron Nitride. Chem. Comm. 51:187–190.

[20] Rafiee M A, Narayanann T N, Hashimn D P, Sakhavand N, Shahsavari R, Vajtai R, Ajayan P M (2013) Hexagonal Boron Nitride and Graphite Oxide Reinforced Multifunctional Porous Cement Composites. Adv. Funct. Mater. 23:5624–5630.

[21] Kubota Y, Watanabe K, Tsuda O, Taniguchi T (2007) Deep Ultraviolet Light-Emitting Hexagonal Boron Nitride Synthesized at Atmospheric Pressure. Science 317:932–934.

[22] Watanabe K, Taniguchi T, Niiyama T, Miya K, Taniguchi M (2009) Far-Ultraviolet Plane-Emission Handheld Device Based on Hexagonal Boron Nitride. Nature Photon. 3:591–594.

[23] Zhang S, Lian G, Si H, Wang J, Zhang X, Wang Q, Cui D (2013) Ultrathin BN Nanosheets with Zigzag

Edge: One-Step Chemical Synthesis, Applications in Wastewater Treatment and Preparation of Highly Thermal-Conductive BN-Polymer Composites. J. Mater. Chem. A. 1:5105–5112.

[24] Yu J, Qin L, Hao Y, Kuang S, Bai X, Chong Y M, Zhang W, Wang E (2010) Vertically Aligned Boron Nitride Nanosheets: Chemical Vapor Synthesis, Ultraviolet Light Emission and Sperhydrophobicity. ACS Nano. 4:414–422.

[25] Yu Y, Chen H, Liu Y, Craig V, Li L H, Chen Y (2014) Superhydrophobic and Superoleophilic Boron Nitride Nanotube-Coated Stainless Steel Meshes for Oil and Water Separation. Adv. Mater. Interf. 1:1300002–1300006.

[26] Lei W, Portehault D, Liu D, Qin S, Chen Y (2013) Porous boron nitride nanosheets for effective water cleaning. Nature Comm. 4:1777–1783.

[27] Li J, Xiao X, Xu X, Lin J, Huang Y, Xue Y, Jin P, Zou J, Tang C (2013) Activated boron nitride as an effective adsorbent for metal ions and organic polluants. Nature 3:3208–3214.

[28] Zhang X, Lian G, Zhang S, Cui D, Wang Q (2012) Boron Nitride Nanocarpets: Controllable Synthesis and their Adsorption Performance to Organic Pollutants. Cryst. Eng. Comm. 14:4670–4676.

[29] Lian G, Zhang X, Si H, Wang J, Cui D, Wang Q (2013) Boron Nitride Ultrathin Fibrous Nanonets: One-Step Synthesis and Applications for Ultrafast Adsorption for Water Treatment and Selective Filtration of Nanoparticles. ACS Appl. Mater. Interf. 5:12773–12778.

[30] Liu D, Lei W, Chen Y (2014) Template-Free Synthesis of Functional 3D BN Architecture for Removal of Dyes from Water. Nature 4:4453–4457.

[31] Lian G, Zhang X, Zhang S, Liu D, Cui D, Wang Q (2012) Controlled Fabrication of Ultrathin-Shell Hollow Spheres with Excellent Performance in Hydrogen Storage and Wastewater Treatment. Energy Environ. Sci. 5:7072–7080.

[32] BJhi S H, Kwon Y K (2004) Hydrogen Adsorption on Boron Nitride Nanotubes: A Path to Room-Temperature Hydrogen Storage. Physic Rev. B 69:245407.

[33] Weng Q, Wang X, Zhi C, Bando Y, Golberg D (2013) Boron Nitride Porous Microbelts for Hydrogen Storage. ACS Nano. 7:1558–1565.

[34] Moussa G, Demirci U B, Malo S, Bernard S, Miele P (2014) Boron Nitride Nanopolyhedrons with Hollow core@mesoporous Shell Structure: From Design to Solid-State Hydrogen Storage Application. J. Mater. Chem. A. 2:7717–7722.

[35] Balmain W H (1842) Bemerkungen über die Bildung von Verbindungen des Bors und Siliciums mit Stickstoff und gewissen Metallen, J. für Praktische Chemie 27:422–430. (In German).

[36] Lipp A, Schwetz K A, Hunold K (1989) Hexagonal Boron Nitride: Fabrication. Properties and Applications. J. Eur. Cera. Soc. 5:3–9.

[37] Lindquist D A, Kodas T T, Smith D M, Xiu X, Hietala S L, Paine R T (1991) Boron Nitride Powders Formed by Aerosol Decomposition of Poly(borazinylamine) Solutions. J. Am. Cera. Soc. 74:3126–3128.

[38] Pruss E A, Wood G L, Kroenke W J, Paine R T (2000) Aerosol Assisted Vapor Synthesis of Spherical Boron Nitride Powders. Chem. Mater. 12:19–21.

[39] Wood G L, Janik J F, Visi M Z, Schubert D M, Paine R T (2005) New Borate Precursors for Boron Nitride Powder Synthesis. Chem. Mater. 17:1855–1859.

[40] Wood G L, Janik J F, Pruss E A, Dreissig D, Kroenke W J, Habereder T, Nöth H, Paine R T (2006) Aerosol Synthesis of Spherical Morphology Boron Nitride Powders from Organoborate Precursors. Chem. Mater. 18:1434–1442.

[41] Wood G L, Paine R T (2006) Aerosol Synthesis of Hollow Spherical Morphology Boron Nitride Particles. Chem. Mater. 18:4716–4718.

[42] Tang C, Bando Y, Golberg D (2002) Large-Scale Synthesis and Structure of Boron Nitride Sub-Micron Spherical Particles. Chem. Comm. 2826–2827.

[43] Tang C, Bando Y, Huang Y, Zhi C, Golberg D (2008) Synthetic Routes and Formation Mechanisms of Spherical Boron Nitride Nanoparticles. Adv. Funct. Mater. 18:3653–3661.

[44] Shi X, Wang S, Yang H, Duan X, Dong X (2008) Fabrication and Characterization of Hexagonal Boron Nitride Powder by Spray Drying and Calcining–Nitriding Technology. J. Solid State Chem. 181:2274–2278.

[45] Lian G, Zhang X, Zhu L, Tan M, Cui D and Wang Q (2010) A Facile Solid State Reaction Route Towards Nearly Monodisperse Hexagonal Boron Nitride Nanoparticles. J. Mater. Chem. 20:3736–3742.

[46] Li Y, Wang Y, Lv Q, Qin Z, Liu X (2013) Synthesis of Uniform Plate-Like Boron Nitride Nanoparticles from Boron Oxide by Ball Milling and Annealing Process. Mater. Lett. 108:96–102.

[47] Xiong C, Tu W (2014) Synthesis of Water-Dispersible Boron Nitride Nanoparticles. Eur. J. Inorg. Chem. 2014:3010–3015.

[48] Hidalgo A, Makarov V, Morell G, Weiner B R. High-Yield Synthesis of Cubic and Hexagonal Boron Nitride Nanoparticles by Laser Chemical Vapor Decomposition of Borazine. Dataset Papers Nanotechnology. 2013; 281672, 5 pages. doi: 10.7167/2013/281672

[49] Salles V, Bernard S, Li J, Brioude A, Chehaidi S, Foucaud S, Miele P (2009) Design of Highly Dense Boron Nitride by the Combination of Spray - Pyrolysis of Borazine and Additive-free Sintering of

Derived Ultrafine Powders. Chem. Mater. 21:2920–2929.

[50] Bernard S, Miele P (2014) Nanostructured and Architectured Boron Nitride. Mater. Today 17:443–450.

[51] Stock A, Pohland E (1926) Borwasserstoffe. IX: $B_3N_3H_6$. Berichte der deutschen chemischen Gesellschaft 59:2215–2223. (In German).

[52] Bechelany M, Bernard S, Brioude A, Stadelmann P, Charcosset C, Fiaty K, Cornu D, Miele P (2007) Synthesis of Boron Nitride Nanotubes by a Template-Assisted Polymer Thermolysis Process. J. Physic Chem. B 111:13378–13384.

[53] Termoss H, Toury B, Pavan S, Brioude A, Bernard S, Cornu D, Valette S, Benayoun S, Miele P (2009) Preparation of Boron Nitride-Based Coatings on Metallic Substrates via Infrared Irradiation of Dip-Coated Polyborazylene. J. Mater. Chem. 19:2671–2674.

[54] Li J, Bernard S, Salles V, Gervais C, Miele P (2010) Preparation of Polyborazylene-Derived Bulk Boron Nitride with Tunable Properties by Warm-Pressing and Pressureless Pyrolysis. Chem. Mater. 22:2010–2019.

[55] Alauzun J G, Ungureanu S, Brun N, Bernard S, Miele P, Backov R, Sanchez C (2011) Novel Monolith-type Boron Nitride Hierarchical Foams Obtained through Integrative Chemistry. J. Mater. Chem. 21:14025–14030.

[56] Schlienger S, Alauzun J, Michaux F, Vidal L, Parmentier J, Gervais C, Babonneau F, Bernard S, Miele P, Parra J B (2012) Micro-, Mesoporous Boron Nitride-Based Materials Templated from Zeolites. Chem. Mater. 24:88–96.

[57] Zhong W, Wang S, Li J, Bechelany M C, Ghisleni R, Rossignol F, Balan C, Chartier T, Bernard S, Miele P (2013) Design of Carbon Fibre Reinforced Boron Nitride Matrix Composites by Vacuum-Assisted Polyborazylene Transfer Moulding and Pyrolysis. J. Eur. Cera. Soc. 33:2979–2992.

[58] Bernard S, Miele P (2014) Polymer-Derived Boron Nitride: A Review on the Chemistry, Shaping and Ceramic Conversion of Borazine Derivatives. Materials 7:7436–7459.

[59] Morell G, Nocua J E, Piazza F, Weiner B R (2009) High-Yield Synthesis of Stoichiometric Boron Nitride Nanostructures. J. Nanomater. 2009: Article ID 429360. 6 pages. 2009. doi:10.1155/2009/429360.

[60] Lourie O R, Jones C R, Bartlett B M, Gibbons, P C Ruoff R S, Buhro W E (2000) CVD Growth of Boron Nitride Nanotubes. Chem. Mater. 12:1808–1810.

[61] Kim M J, Chatterjee S, Kim S M, Stach E A, Bradley M G, Pender M J, Sneddon L G, Maruyama B (2008) Double Walled Boron Nitride Nanotubes Grown by Floating Catalyst Chemical Vapor Deposition. Nano. Lett. 8:3298–3302.

[62] Nagashima A, Tejima N, Gamou Y, Kawai T, Oshima C (1995) Electronic Dispersion Relations of Monolayer Hexagonal Boron Nitride Formed on the Ni(111) Surface. Physic Rev. B 51:4606–4613.

[63] Corso M, Auwärter W, Muntwiler M, Tamai A, Greber T, Osterwalder J (2004) Boron nitride nanomesh. Science 303:217–220.

[64] Berner S, Corso M, Widmer R, Groening O, Laskowski R, Blaha P, Schwarz K, Goriachko A, Over H, Gsell S, Schreck M, Sachdev H, Greber T, Osterwalder J (2007) Boron Nitride Nanomesh: Functionality from a Corrugated Monolayer. Angewandte Chemie Int. Edn. 46:5115–5119.

[65] Ye Y, Graupner U, Krüger R (2012) Deposition of Hexagonal Boron Nitride from N-Trimethylborazine (TMB) for Continuous CVD Coating of SiBNC Fibers. Chem. Vapor Deposit. 17:249–255.

[66] Bernard S, Salles V, Li J, Brioude A, Bechelany M, Demirci U B, Miele P (2011) High-Yield Synthesis of Hollow Boron Nitride Nano-Polyhedrons. J. Mater. Chem. 21:8694–8699.

[67] Salles V, Bernard S, Chiriac R, Miele P (2012) Structural and Thermal Properties of Boron Nitride Nanoparticles. J. Eur. Cera. Soc. 32:1867–1871.

[68] Wideman T, Sneddon L G (1995) Convenient Procedures for the Laboratory Preparation of Borazine. Inorg. Chem. 34:1002–1003.

[69] Gmelin Handbuch der Anorganishen Chemie, Borazine and Its Derivatives; Springer-Verlag: New York, 1978; Vol. 51.

[70] Bernard S, Ayadi K, Létoffé J M, Chassagneux F, Berthet M P, Cornu D, Miele P (2004) Evolution of Structural Features and Mechanical Properties During the Conversion of Poly[(methylamino)borazine] Fibers into Boron Nitride Fibers. J. Solid State Chem. 177:1803–1810.

[71] Kartha V B, Krishnamachari S L N G, Subramaniam C R (1967) The Infrared Spectra of Borazine and its Isotopic Species. Assignment of the a''_2 Fundamental Modes. J. Mol. Spectroscopy. 23:149–157.

[72] Pease R S (1952) An X-Ray Study of Boron Nitride. Acta Crystallographica 5:356–361.

[73] Thomas Jr J, Weston N E, O'Connor T E (1963) Turbostratic Boron Nitride, Thermal Transformation to Ordered-Layer-Lattice Boron Nitride. J. Am. Chem. Soc. 84:4619–4622.

[74] Toutois P, Miele P, Jacques S, Cornu D, Bernard S (2006) Structural and Mechanical Behavior of Boron Nitride Fibers Derived from Poly[(Methylamino)Borazine] Precursors: Optimization of the Curing and Pyrolysis Procedures. J. Am. Cera. Soc. 89:42–49.

[75] Salles V, Bernard S, Brioude A, Cornu D, Miele P (2010) A New Class of Boron Nitride Fibers with Tunable Properties by Combining an Electrospin-

ning Process and the Polymer-Derived Ceramics Route. Nanoscale 2:215–217.

[76] Gervais C, Maquet J, Babonneau F, Duriez C, Framery E, Vaultier M, Florian P, Massiot D (2001) Chemically Derived BN Ceramics: Extensive 11B and 15N Solid-State NMR Study of a Preceramic Polyborazilene. Chem. Mater. 13:1700–1707.

[77] Irwin A D, Holmgren J S, Jonas J (1998) Solid State ^{29}Si and ^{11}B NMR Studies of Sol-Gel Derived Borosilicates. J. Non-Crystal Solids 101:249–254.

[78] Kim S Y, Park J, Choi H C, Ahn J P, Hou J Q, Kang H S (2007) X-Ray Photoelectron Spectrocopy and First Principles Calculation of BCN Nanotubes. J. Am. Chem. Soc. 129:1705–1716.

[79] Bernard S, Chassagneux F, Berthet M P, Cornu D, Miele P (2005) Crystallinity, Crystalline Quality and Microstructural Ordering in Boron Nitride Fibers. J. Am. Cera. Soc. 88:1607-14.

[80] Bernard S, Chassagneux F, Berthet M P, Vincent H, Bouix J (2002) Structural and Mechanical Properties of a High-Performance BN fibre. J. Eur. Cera. Soc. 22:2047–2059.

[81] Toury B, Bernard S, Cornu D, Chassagneux F, Létoffé J M, Miele P (2003) High-Performances Boron Nitride Fibers Obtained from Asymmetric Alkylaminoborazine. J. Mater. Chem. 13:274–279.

[82] Sing K S W, Everett D H, Haul R A W, Moscou L, Pierotti R A, Rouquerol J, Siemieniewska T (1985) Reporting Physisorption Data for Gas/Solid Systems with Special Reference to the Determination of Surface Area and Porosity. Pure Appl. Chem. 57:603–619.

[83] Rouquerol J, Avnir D, Fairbridge C W, Everett D H, Haynes J M, Pernicone N, Ramsay J D F, Sing K S W, Unger K K (1994) Recommendations for the Characterization of Porous Solids (Technical Report) Pure Appl. Chem. 66:1739–1758.

[84] Pan Y, Huo K, Hu Y, Fu J, Lu Y, Dai Z, Hu Z, Chen Y (2005) BN nanocages synthesized by a moderate thermochemical approach. Small 1:1199–1203.

[85] Zhu Y C, Bando Y, Yin L W, Golberg D (2004) Hollow Boron Nitride (BN) Nanocages and BN-Nanocage-Encapsulated Nanocrystal. Chem. Eur. J. 10:3667–3672.

[86] Hirano T, Oku T, Suganuma K (1999) Formation of Gold and Iron Oxide Nanoparticles Encapsulated in Boron Nitride Sheets. J. Mater. Chem. 9:855–857.

[87] Oku T, Kusunose T, Niihara K, Suganuma K (2000) Chemical Synthesis of Silver Nanoparticles Encapsulated in Boron Nitride Nanocages. J. Mater. Chem. 10:255–257.

[88] Komatsu S, Shimizu Y, Moriyoshi Y, Okada K, Mitomo M (2001) Nanoparticles and Nanoballoons of Amorphous Boron Coated with Crystalline Boron Nitride. Appl. Physic Lett. 79:188–190.

[89] Yeadon M, Lin M, Loh K P, Boothroyd B, Fu J, Hu Z (2003) Direct Observation of Boron Nitride Nanocage Growth by Molecular Beam Nitridation and Liquid-Like Motion of Fe–B Nanoparticles. J. Mater. Chem. 13:2573–2576.

[90] Gleiman S, Chen C K, Datye A (2002) Melting and Spheroidization of Hexagonal Boron Nitride in a Microwave-Powered, Atmospheric Pressure Nitrogen Plasma. J. Mater. Chem. 37:3429–3440.

[91] David L, Bernard S, Gervais C, Miele P, Singh G (2015) High Capacity and Rate Capability of SiCN/BN Nanosheet Composite as Li-ion Battery Electrode. J. Physic Chem. C 119:2783–2791.